



Rapid thermal sensors with high resolution based on an adaptive dual-comb system*

Yi-zheng GUO^{†1}, Ming YAN², Qiang HAO¹, Kang-wen YANG¹, Xu-ling SHEN^{†1,2,3}, He-ping ZENG^{††1,2}

¹Shanghai Key Laboratory of Modern Optical System, Engineering Research Center of Optical Instrument and System (Ministry of Education), School of Optical-Electrical and Computer Engineering, University of Shanghai for Science and Technology, Shanghai 200093, China

²State Key Laboratory of Precision Spectroscopy, East China Normal University, Shanghai 200062, China

³Shanghai Institute of Optics and Fine Mechanics, Chinese Academy of Sciences, Shanghai 201800, China

[†]E-mail: yizhengguo_usst@126.com; xlshen@lps.ecnu.edu.cn; hpzeng@phy.ecnu.edu.cn

Received June 1, 2018; Revision accepted Jan. 17, 2019; Crosschecked May 13, 2019

Abstract: We report a high-resolution rapid thermal sensing based on adaptive dual comb spectroscopy interrogated with a phase-shifted fiber Bragg grating (PFBG). In comparison with traditional dual-comb systems, adaptive dual-comb spectroscopy is extremely simplified by removing the requirement of strict phase-locking feedback loops from the dual-comb configuration. Instead, two free-running fiber lasers are adopted as the light sources. Because of good compensation of fast instabilities with adaptive techniques, the optical response of the PFBG is precisely characterized through a fast Fourier transform of the interferograms in the time domain. Single-shot acquisition can be accomplished rapidly within tens of milliseconds at a spectral resolution of 0.1 pm, corresponding to a thermal measurement resolution of 0.01 °C. The optical spectral bandwidth of the measurement also exceeds 14 nm, which indicates a large dynamic temperature range. It shows great potential for thermal sensing in practical outdoor applications with a loose self-control scheme in the adaptive dual-comb system.

Key words: Interferometers; Fiber sensors; Laser spectroscopy
<https://doi.org/10.1631/FITEE.1800347>

CLC number: O439

1 Introduction

Because of their outstanding advantages of small size, low cost, high resolution, multiplexing capability, and immunity to electromagnetic interference, fiber Bragg gratings (FBGs) have been widely used for high-sensitivity strain measurements in industrial applications such as geophysical surveys and civil engineering in structure monitoring (Measures, 2001;

Cusano et al., 2004; Majumder et al., 2008). Compared with dynamic systems for signals above 10 Hz, quasi-static signals with frequencies below 10 Hz are of more interest for slowly varying signals such as temperature, seismic and volcanic motion (He et al., 2012). Though ultra-high resolution has been achieved in the field of dynamic sensing (Udem et al., 2002; He et al., 2012; Li et al., 2013). There are still challenges in static sensing in that resolution at low frequency is always degraded by frequency noise from the laser source. Generally, the transmission or reflection spectrum shift induced by the deformation of the Bragg grating structure can be detected by an optical spectrometer (Wu et al., 2010). To achieve high resolution in static strain sensing, single-longitudinal-mode continuous-wave (CW) lasers phase-locked on frequency references such as Fabry-

[‡] Corresponding author

* Project supported by the National Instrumentation Program (No. 2012YQ150092), the China Postdoctoral Science Foundation (No. 2015M581634), the National Natural Science Foundation of China (No. 11704253), and the Shanghai Youth Science and Technology Talent Sailing Program (No. 17YF1413100)

ORCID: Yi-zheng GUO, <http://orcid.org/0000-0002-9153-3050>

© Zhejiang University and Springer-Verlag GmbH Germany, part of Springer Nature 2019

Perot (FP) cavities or frequency combs are often adopted to detect the spectral shift of FBGs (Kersey et al., 1993; Du et al., 1999; Chow et al., 2005; Gagliardi et al., 2010; Lam et al., 2010a, 2010b). Even with high resolution in static sensing, the system still encounters challenges in stability and practicability with bulky and complex CW systems. Furthermore, the limitation of the available dynamic range and multiplexing capability sourced from the narrow tunable wavelength range of stabilized CW lasers is insufficient to meet the general requirements in a wide range of geophysical applications (Kuse et al., 2012). Robust, compact, precise, and fast interrogation systems are needed. In general, precision and long-term stability of a quasi-static strain system are determined by the suppression of laser frequency noise (Chow et al., 2005; Schliesser et al., 2005).

Optical combs with a large number of discrete optical frequencies pave the way for overcoming the difficulties in narrow spectral spans (Udem et al., 2009; Zolot et al., 2012). In the past decades, optical combs have been dramatically simplified and improved the accuracy of frequency metrology with advantages in precisely measuring frequencies of light (Yasui et al., 2006; Newbury and Swann, 2007). Fiber-laser frequency combs are of particular importance for telecommunications and optical sensing applications (Coddington et al., 2009; Taurand et al., 2010). Traditionally, fast Fourier transform (FFT) spectroscopy has been an essential and powerful tool for molecular absorption spectroscopy (Coddington et al., 2008; Bernhardt et al., 2010; Deschênes, 2010). Due to the maximum displacement of the movable mirror in the interferometer, the resolution is at a level of 100 MHz with the acquisition time of several hours (Rieker et al., 2014). The technique of traditional Fourier transform spectroscopy is limited by the velocity of scanning components. However, with the combination of two frequency combs in an interferometric setup as a dual-comb system, higher resolution and faster acquisition over a broad spectral span can be achieved (Schiller, 2002; Newbury et al., 2010; Droste et al., 2016). Although frequency mode spacing is unresolved by a conventional optical spectrometer, precise and broadband characterization of FBG sensors can be achieved by employing dual-comb spectroscopy (DCS) (Schiller, 2002; Keilmann et al., 2004; Coddington et al., 2010). Resolution of

34 ne with a large dynamic range of about 1 THz and multiplexing capability is ensured in the detection of the FBG spectrum in the static regime (Kuse et al., 2013). The DCS concept is realized by the generation of a radio-frequency comb composed of distinguishable heterodyne beats between optical combs. Compared with conventional Fourier transform spectroscopy, DCS has advantages in high acquisition speed, broader spectral coverage, high signal-to-noise ratio (SNR), high sensitivity, and high resolution (Diddams, 2010; Coddington et al., 2016). DCS holds much promise in practical applications such as outdoor and industrial applications. As an essential and powerful tool for molecular absorption spectroscopy, optical frequency combs can be realized using many approaches. Commonly, combs fully stabilized at ultra-stable CW lasers by active feedbacks are taken as the light source (Keilmann et al., 2004; Washburn et al., 2004; Deng et al., 2005; Coddington et al., 2008, 2010; Bernhardt et al., 2010; Zhang et al., 2013; Zhu et al., 2013). Achieving long mutual coherence time demands high stability in the active feedback circuits for the control of repetition rates and carrier-enveloped offset (CEO) frequencies. The complexity of the system is also increased by the unavoidable detection of the CEO signals. It militates against a simple and easy-to-operate interrogation system of FBGs because of the strict phase-locking feedback loop requirements to preserve the resolution. It also needs significant effort to improve the width of comb lines in case the spectra are spoiled when averaging over time of seconds or minutes for higher resolution (Kourogi et al., 1993; Bernhardt et al., 2010). To solve the problem, post processing and real-time digital phase correction can be achieved by complicated programming with the field-programmable gate array (Giaccari et al., 2008; Roy et al., 2012; Jin et al., 2015). Mutual coherence times of the order of seconds are attained by another novel technique based on analog adaptive sampling (Ideguchi et al., 2012, 2014; Cassinerio et al., 2014; Yasui et al., 2015). Techniques of DCS are seriously limited by slow drift with low-frequency noise in practical applications. To fully benefit from longer acquisition time, laser oscillators need to be stabilized to a standard reference as combs. An all-optical scheme of dual-comb spectroscopy is also reported as a practical low-complexity dual-comb metrology technique. Pulse trains have passive

mutual coherence due to the common-mode noise cancellation in a shared single cavity (Ideguchi et al., 2016; Zhao et al., 2016). However, uncontrollable slight slow drifts exist with environmental variation. DCS based on electro-optic modulators is a good choice, but the acquisition time is limited by the narrow spectral bandwidth being broadened in non-linear fiber (Millot et al., 2016; Yan et al., 2017). The high stability of a CW laser is still required and achieved by isolating it from the environment. Constant temperature control of an on-chip dual-comb system based on quantum cascade lasers (QCLs) is an ideal method to realize long-term operation of dual-comb spectroscopy. Because of the gain recovery time, the resolution is limited at GHz with QCLs (Hugi et al., 2012). The systems mentioned above all suffer from slow dynamics sourced from long-term environmental deviations as low-frequency noises. It tells against the long-term operation of the dual-comb system that invalid active compensations occur with distortions or even out-band suppression loss of signals. Specifically, in the adaptive sampling technique, long-term operation of the dual-comb system is hindered by more serious problems in slow drifts due to the totally free-running oscillators. By removing slow drifts, it has great potential in outdoor applications due to the well adapted compensations of fast instabilities between comb lines without strict phase-locking. Passive temperature stabilization for combs is always adopted to reduce the slow drifts induced by temperature variations. However, the control results are not always good enough using single-loop direct temperature control because of the high sensitivity of combs to the surrounding temperature and the actual control accuracy of temperature stabilization. Effective control of low-frequency noise to dual-comb systems will promote further practical industrial applications. With the developments of techniques in optical combs, a compact, light, portable, and integrated dual-comb system will be popular in outdoor applications.

In this paper, we present a method based on adaptive sampling techniques to rapidly and precisely measure the optical frequency shifts of a PFBG in the radio-frequency domain. Low-frequency noises from the dual-comb system are effectively suppressed by self-control schemes on slow drifts. The system exhibits high precision and long-term stability due to the

compensation of fast instabilities and loose stabilization on comb lines. It holds much promise for practical outdoor application.

2 Adaptive dual-comb spectroscopy

2.1 Experimental setup

The experimental setup of the adaptive dual-comb spectroscopy (ADCS) is shown in Fig. 1. Seed pulses from two self-starting SESAM-mode-locked PM erbium-doped fiber lasers are amplified to 50 mW by pre-amplifiers and then divided into two parts by couplers with a coupler ratio of 20:80. Twenty percent are delivered into a network consisting of couplers with a coupler ratio of 50:50 for adaptive signal generation from beat signals between combs and CW lasers (RIO ORIONTM). The average output power of CW lasers centered at 1550 nm and 1564 nm is 10 mW. The spectral linewidth of CW lasers is less than 3 kHz. Beat signals detected by four photodiodes (PD1–PD4) are delivered into the RF processing module. The other 80% are injected into two 10-cm HNLFs to generate proper optical wave bands for applications. Appropriate spectra are filtered for sampling by two fiber-tailed band-pass filters. The filtered lasers in one path are aligned into the gas cell from fibers by a collimator. After the gas cell, lasers are coupled into fibers by the second collimator and combined with the filtered lasers in another path for interferogram signal generation. Interferogram signals detected by an InGaAs fast photodiode (PD5) are transferred into the RF signal processing module for further compensation of the instabilities of comb lines. In the cavity of the fiber lasers, the compact structure is beneficial for the reduction of disturbance from the environment. The wavelength division multiplexer (WDM), isolator (ISO), and TAP are integrated. Collimators in delay lines for repetition rate match between combs are fixed and packaged after light path alignments. Due to the all PM fiber operation of the oscillators, a half wave plate (HWP) is needed to keep the lasers in the PM state during alignment. The integration of SESAM and the circulator makes it easier to connect with the cavity. The SESAM we use has a modulation depth of 13% and a non-saturable loss of 9%. A PZT is also stuck with a piece of intra-cavity fibers to stretch the cavity length by applying driving

voltages. To control the temperature of the combs, entire components and fibers of oscillators are evenly close to the surface of a thermoelectric cooler (TEC) device (Shen et al., 2018). Heat insulation materials are applied to the oscillators to ensure that the only main approach of heat transfer between oscillators and environment is the TEC.

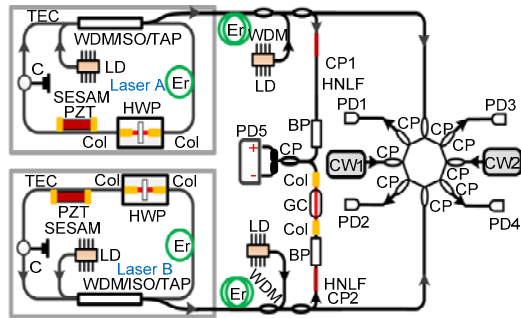


Fig. 1 Experimental setup

LD, laser diode at 980 nm; ISO, isolator; WDM, wavelength division multiplexer; SESAM, semiconductor saturable absorber mirror; HWP, half wave plate; Col, collimator; GC, gas cell; TEC, thermoelectric cooler; PZT, piezoelectric ceramics; Er, erbium-doped fiber; CW1, continuous wave laser centered at 1550 nm; CW2, continuous wave laser centered at 1564 nm; HNLf, high nonlinear fiber; CP, fiber coupler; PD1–PD4, photodiodes; PD5, balanced detector; BP, bandpass filter

2.2 Sampling theorem

Traditionally, in the time domain interferogram signals of a dual-comb system with tight phase locking of comb lines can be directly sampled in the analog-to-digital conversion with a constant external clock rate, which meets Nyquist’s theorem. The spectral information can be well retrieved by an FFT of the sampled interferogram signals in the frequency domain. However, in our adaptive dual-comb system, interferogram signals fluctuate because of the free-running oscillators. Apparently, serious distortions will be induced by direct sampling of interferogram signals with a constant external clock rate. With adaptive sampling techniques, interferogram signals are sampled with a nonconstant external clock rate. Spectral information is also well retrieved with FFT by good compensation of instabilities of comb lines. To understand the mechanism of adaptive dual-comb spectroscopy, we first focus on the relationships between the external clocks and signals. According to Nyquist’s theorem, the clock frequency f_2 should be at

least f_1 . In the simplest situation, f_1 and f_2 are constant frequencies (Fig. 2).

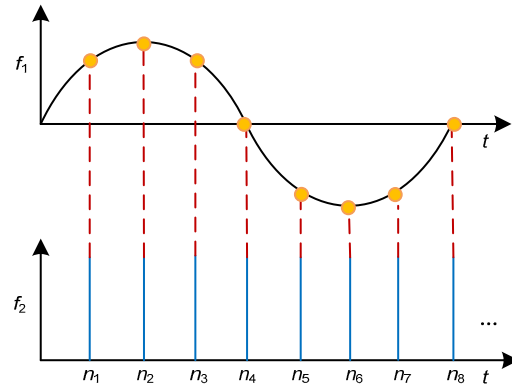


Fig. 2 Illustration of signal f_1 sampling at clock signal f_2

In Fig. 2, signal f_1 is sampled at the edges of clock signal f_2 . The relationship between the number of sampling points and the sampling frequency is described by

$$n-1=f_2/f_1, \tag{1}$$

where n is the number of sampling points. In this way, the period of the sampled signal can be expressed as

$$T=(n-1)\cdot\tau, \tag{2}$$

where $\tau=1/f_2$ is the period of the sampling clock. Then the retrieved signal frequency can be expressed as

$$F=\frac{1}{T}=\frac{f_1}{f_2}\cdot\frac{1}{\tau}. \tag{3}$$

Clearly, $1/\tau$ is the fixed clock signal f_2 . The processed signal frequency can be expressed as

$$F=\frac{f_1}{f_2}\cdot f_0=f_1. \tag{4}$$

Certainly, the retrieved signal frequency is equal to the original signal frequency. It definitely indicates the feasibility of the dual-comb spectroscopy with constant sampling clock. However, in a more complex situation such as an adaptive dual-comb system, the retrieved signal frequency is often distorted, because of the time-varying signals f_1 and clock signals f_2 . The relationship between the retrieved signal

frequency and the original signal frequency can be studied based on Eq. (4). We assume that the small variations of signals f_1 and f_2 during the sampling are δ_1 and δ_2 , respectively. The retrieved frequency of the varying signal can be expressed by the following equation:

$$F' = \frac{f_1 + \delta_1}{f_2 + \delta_2} \cdot f_0, \quad (5)$$

where f_0 is a constant clock frequency applied during FFT processing. According to Eq. (5), it seems that the retrieved signal frequency is related to the variations of f_1 and f_2 . Generally, the retrieved signal frequency F' is also a variable. It also explains the distortions of retrieved signals in the adaptive dual-comb system with constant sampling clock rates. There is still a chance to attain a constant retrieved signal frequency when f_1 and f_2 are linear, as in Eqs. (6) and (7):

$$f_1 = k_1 \cdot \Delta f, \quad (6)$$

$$f_2 = k_2 \cdot \Delta f. \quad (7)$$

δ_1 and δ_2 can also be expressed as

$$\delta_1 = k_1 \cdot (\Delta f + \delta), \quad (8)$$

$$\delta_2 = k_2 \cdot (\Delta f + \delta). \quad (9)$$

With such formulae, the retrieved signal frequency can be expressed as

$$F' = \frac{1}{T'} = \frac{f_1 + \delta_1}{f_2 + \delta_2} \cdot f_0 = \frac{k_1}{k_2} \cdot f_2. \quad (10)$$

In this case, the retrieved signal frequency can be constant. Fortunately, it offers an opportunity to retrieve stable frequency components from interferograms of the free-running dual-comb system. The advantages of a tight phase-locking dual-comb system can be kept in an adaptive dual-comb system. In Section 2.3, we will describe in detail how fast instabilities between “combs” lines are well compensated for by adaptive sampling techniques.

2.3 Adaptive sampling techniques

As shown in Fig. 1, the pulse lasers and CW lasers are named laser A, laser B, CW50, and CW64,

respectively. In the adaptive dual-comb system setup, CW lasers and pulse lasers are combined for adaptive signal generation. The corresponding beat notes between pulse lasers and CW lasers are named 50A, 50B, 64A, and 64B. For convenience of description, lasers are illustrated in the frequency domain (Fig. 3). Comb A and comb B have comb lines spaced at the repetition frequencies of pulsed lasers A and B, respectively. CW64 and CW50 are the optical frequency positions corresponding to 1564 nm and 1550 nm, respectively. The spectral region is filtered as frequency components of the interferograms.

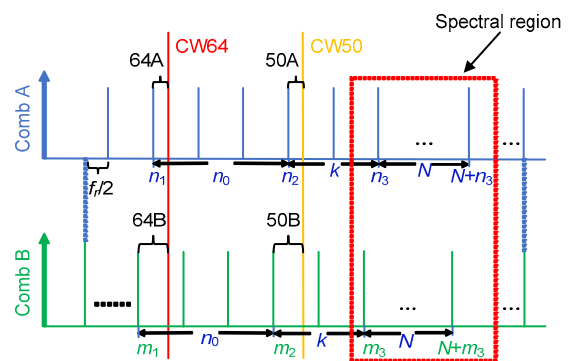


Fig. 3 Lasers in the frequency domain

As shown in Fig. 3, the optical frequency positions are tuned properly by adjusting the repetition rate difference of the pulse lasers. In this case, coefficient numbers of comb lines must have the following relationship:

$$\begin{cases} m_1 - n_1 = m_2 - n_2 = m_3 - n_3, \\ n_2 - n_1 = m_2 - m_1 = n_0, \\ n_3 - n_2 = m_3 - m_2 = k, \end{cases} \quad (11)$$

where $n_1, n_2, n_3, m_1, m_2,$ and m_3 are integers, and n_0 and k are the corresponding sequence number differences of comb teeth. According to the characteristics of an optical comb, the comb line in the frequency domain can be expressed as

$$f_a = n \cdot f_{rA} + f_{ceo a}, \quad (12)$$

$$f_b = n \cdot f_{rB} + f_{ceo b}, \quad (13)$$

where f_{rA} and f_{rB} are repetition rates of lasers A and B, respectively. n and m are integers, and the carrier-envelope-phase offset frequencies are $f_{ceo a}$ and $f_{ceo b}$. According to Eqs. (12) and (13), the frequency

components in the box in Fig. 3 can be expressed as

$$\begin{cases} f_{\text{Beat}1} = n_3 \cdot f_{\text{rA}} - m_3 \cdot f_{\text{rB}} + \Delta f_{\text{ceo}}, \\ f_{\text{Beat}2} = (n_3 + 1) \cdot f_{\text{rA}} - (m_3 + 1) \cdot f_{\text{rB}} + \Delta f_{\text{ceo}}, \\ \dots \\ f_{\text{Beat}(N+1)} = (n_3 + N) \cdot f_{\text{rA}} - (m_3 + N) \cdot f_{\text{rB}} + \Delta f_{\text{ceo}}, \end{cases} \quad (14)$$

where n_3 and m_3 are integers, Δf_{ceo} is the difference of the carrier-envelope-phase offset frequency between laser A and laser B. We assume that there are N lines in the box region in Fig. 3.

The beats between pulse lasers and CW lasers can be expressed as follows:

$$f_{50A} = f_{50} - (n_2 \cdot f_{\text{rA}} + f_{\text{ceo}a}), \quad (15)$$

$$f_{50B} = f_{50} - (m_2 \cdot f_{\text{rB}} + f_{\text{ceo}b}), \quad (16)$$

$$f_{64A} = f_{64} - (n_1 \cdot f_{\text{rA}} + f_{\text{ceo}a}), \quad (17)$$

$$f_{64B} = f_{64} - (m_1 \cdot f_{\text{rB}} + f_{\text{ceo}b}), \quad (18)$$

where f_{50} and f_{64} are the optical frequencies of CW50 and CW64, respectively. n_1 , n_2 , m_1 , and m_2 are integers. $f_{\text{ceo}a}$ and $f_{\text{ceo}b}$ are the CEO drifts of the corresponding lasers. In our experiment, f_{50A} , f_{50B} , f_{64A} , and f_{64B} are set to around 10, 20, 10, and 25 MHz, respectively. Adaptive signals (AS1 and AS2) are generated through processing these four original signals by mixing, filtering, multiplication, etc. A radio-frequency processing circuit module is applied to compensate for the fast instabilities of comb lines (Fig. 4).

Four original beat notes are first filtered and amplified properly. To match the commercial filters, appropriate frequency shifting is applied in f_{50B} and f_{64A} as shown in the following expressions:

$$\begin{cases} f_{50B2} = f_{50} - (m_2 \cdot f_{\text{rB}} + f_{\text{ceo}b}) + f_{10M}, \\ f_{64B2} = f_{64} - (m_1 \cdot f_{\text{rB}} + f_{\text{ceo}b}) + f_{15M}. \end{cases} \quad (19)$$

Secondly, f_{50B2} is mixed with f_{50A} to eliminate the CW50 frequency component and f_{64B2} is mixed with f_{64A} to eliminate the CW64 frequency component. The results are named f_{S1} and f_{S2} , expressed as

$$\begin{cases} f_{S1} = f_{50B2} - f_{50A} = n_2 \cdot f_{\text{rA}} - m_2 \cdot f_{\text{rB}} + \Delta f_{\text{ceo}} + f_{10M}, \\ f_{S2} = f_{64B2} - f_{64A} = n_1 \cdot f_{\text{rA}} - m_1 \cdot f_{\text{rB}} + \Delta f_{\text{ceo}} + f_{15M}. \end{cases} \quad (20)$$

f_{S1} and f_{S2} are 20 and 30 MHz, respectively. Term Δf_{ceo} is contained in both f_{S1} and f_{S2} . To obtain f_{S3} , we mix f_{S1} and f_{S2} . It can be expressed as

$$f_{S3} = f_{S2} - f_{S1} = (m_2 - m_1) f_{\text{rB}} - (n_2 - n_1) f_{\text{rA}} + f_{5M}. \quad (21)$$

According to Eq. (11), it can be reduced by further frequency shifting of 5 MHz and multiplexing of 16:

$$f_{\text{AS}2} = 16 \cdot n_0 \cdot \Delta f. \quad (22)$$

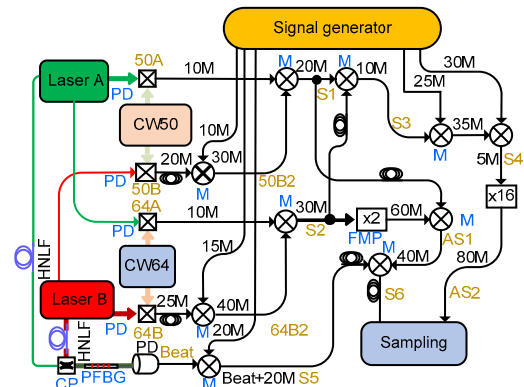


Fig. 4 Processing circuit

Laser A, pulse laser A; laser B, pulse laser B; CW50, continuous wave laser centered at 1550 nm; CW64, continuous wave laser centered at 1564 nm; HNLf, high nonlinear fiber; PD, photodiode; FMP, frequency multiplier; M, mixer; CP, fiber coupler

To obtain $f_{\text{AS}1}$, we operate Eq. (20) as $2f_{S2} - f_{S1}$. It can be expressed by

$$f_{\text{AS}1} = (2n_1 - n_2) f_{\text{rA}} - (2m_1 - m_2) f_{\text{rB}} + \Delta f_{\text{ceo}} + f_{20M}. \quad (23)$$

By mixing a fixed frequency shift of 20 MHz in Eq. (14) and mixing $f_{\text{AS}1}$, Δf_{ceo} is eliminated in low frequency components. The compensated new frequency components can be expressed as

$$\begin{cases} f_{\text{SS_Beat}1} = (n_3 + n_2 - 2n_1) f_{\text{rA}} - (m_3 + m_2 - 2m_1) f_{\text{rB}}, \\ f_{\text{SS_Beat}2} = (n_3 + n_2 - 2n_1 + 1) f_{\text{rA}} \\ \quad - (m_3 + m_2 - 2m_1 + 1) f_{\text{rB}}, \\ f_{\text{SS_Beat}(N+1)} = (n_3 + n_2 - 2n_1 + N) f_{\text{rA}} \\ \quad - (m_3 + m_2 - 2m_1 + N) f_{\text{rB}}. \end{cases} \quad (24)$$

According to Eq. (11), Eq. (24) can be expressed as

$$\begin{cases} f_{S6_Beat1} = (2n_0 + k) \cdot \Delta f, \\ f_{S6_Beat2} = (2n_0 + k + 1) \cdot \Delta f, \\ \dots \\ f_{S6_Beat(N+1)} = (2n_0 + k + N) \cdot \Delta f. \end{cases} \quad (25)$$

Considering the same formula forms of Eqs. (6) and (7) with f_{AS1} and f_{AS2} , stable retrieved frequency components can be attained according to Eq. (10):

$$\begin{cases} F'_{S6_Beat1} = (2n_0 + k) \cdot f_0 / (16n_0), \\ F'_{S6_Beat2} = (2n_0 + k + 1) \cdot f_0 / (16n_0), \\ \dots \\ F'_{S6_Beat(N+1)} = (2n_0 + k + N) \cdot f_0 / (16n_0), \end{cases} \quad (26)$$

where n_0 , k , and N are all integers.

3 Results

3.1 Experimental setup of rapid thermal sensors

The principle of ADCS mentioned above shows that short-term instabilities in both timing fluctuations and phase fluctuations between combs are well cancelled with adaptive signals during signal processing. Amplitude modulation on comb lines from gas absorption lines can be well retrieved by the FFT of the interferograms when the gas cell is inserted in one optical path as shown in Fig. 1. Based on the ADCS, the outputs of laser A and laser B are divided into two parts by couplers with a ratio of 20:80. Twenty percent is injected into the ADCS to generate adaptive signals (Fig. 5). To satisfy different wavelength requirements in applications, a supercontinuum is generated in the high nonlinear fiber after injecting 80% of the pulse laser (Fig. 6). The two supercontinua are coupled by couplers with a ratio of 50:50. The proper wave band is filtered by a band-pass filter to interrogate a phase-shifted fiber Bragg grating (PFBG) as fast thermal sensing. We attached PFBG to the TEC and insulated the PFBG from the surrounding environment with insulation. Rapid thermal sensing at high resolution was achieved by controlling the change in TEC temperature. We collected the interference pattern through the data acquisition card (DAQ) and analyzed the moving relationship between the temperature and the peak frequency of the PFBG center through data processing.

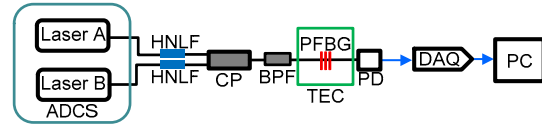


Fig. 5 Experimental setup

Laser A, pulse laser A; laser B, pulse laser B; HNLF, high nonlinear fiber; PD, balanced detector; CP, fiber coupler; BPF, band-pass filter; TEC, thermoelectric cooler; PFBG, phase-shifted fiber Bragg grating; DAQ, data acquisition; PC, computer

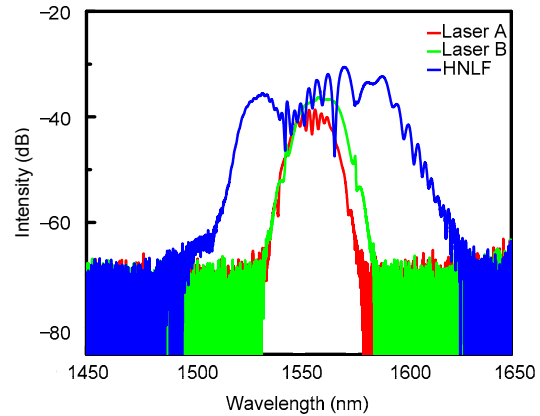


Fig. 6 Spectra of laser A and laser B and broadened spectrum in HNLF

3.2 Fiber Bragg grating sensing

According to the fiber Bragg grating equation

$$\lambda_B = 2n_{\text{eff}}\Lambda, \quad (27)$$

where λ_B is the center wavelength of the fiber Bragg grating, n_{eff} is the effective refractive index of the grating, and Λ is the grating period, the optical response of fiber Bragg grating is related to n_{eff} and Λ , which are sensitive to the surrounding environment such as temperature and pressure. On the other hand, fiber Bragg gratings can be used as sensitive sensors by precisely characterizing their optical response. In our experiment, a PFBG is used as a thermal sensor with zero pressure. To study the temperature response, the PFBG is evenly placed on the surface of a TEC which has a temperature control resolution better than 0.01 °C.

3.3 Data processing

The analogue-to-digital conversion is accomplished in the data acquisition card, and the data is stored on the computer hard drive. With a set of

programs in Matlab, further treatment and analysis of the resulting spectra will exhibit precise relationships between the optical response of the PFBG and temperature as thermal sensors. The digitizer (ATS9462, AlazarTech) has 65 MHz bandwidth and a sampling rate of up to 1.8×10^8 samples/s. Its specified dynamic range is 16 bits. The internal memory of the digitizer is 2^{28} samples. This currently limits the duration of an acquisition at a sampling rate of 80 MHz to 3.3 s. The digitizer possesses an external clock input, which enables synchronization between data acquisition and the adaptive signals f_{AS2} .

Single-shot acquisition is accomplished within 104 ms with 6.3 MHz apodized optical resolution at a refresh rate of 180 Hz (Fig. 7). The TEC temperature is set at 23 °C. The internal memory is 2^{23} samples. The interferograms are Fourier-transformed as radio-frequency spectra in the frequency domain. The signal-to-noise ratio estimated from the root-mean-square noise in a single-shot acquisition is about 18, which is approximately the same as the one in Ideguchi et al. (2014). It exhibits the potential in good spectral coherence and comb line correlations even after nonlinear spectrum broadening. The spectral SNR of 350 is obtained by averaging 500 sets of data (Fig. 8). The key characteristic of PFBG is the existence of transmission windows with a 3-dB optical bandwidth of 7 pm at the reflection band, resulting in high wavelength selectivity. As shown in Fig. 8, both side wings and the deep notch of PFBG are finely depicted by comb lines in the radio-frequency domain from 9.9 to 10.2 MHz. As shown in the insertion, resolvable comb lines with 8-Hz 3-dB bandwidth in the radio-frequency domain are spaced at 180 Hz.

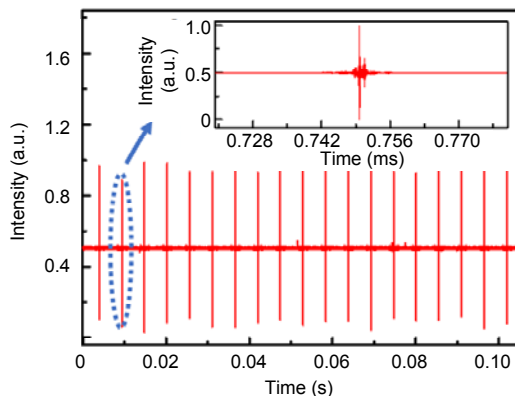


Fig. 7 104-ms sampled interferometric electric signals (insertion: details of single interferometric electric signals with a span of 50 ms)

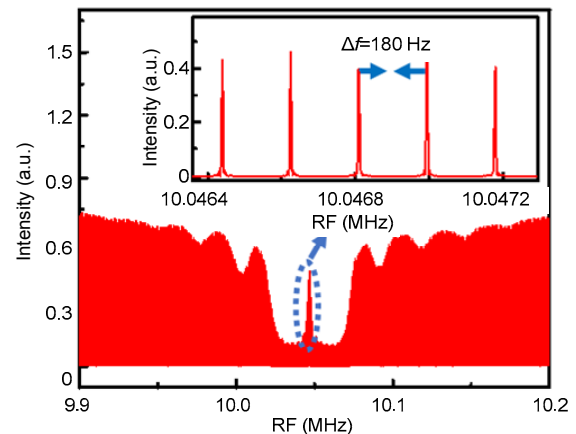


Fig. 8 Spectral profile of the PFBG (insertion: resolvable comb lines in transmission windows at the reflection band)

Given the resolution required in practical applications, a different acquisition time is needed. As shown in the insertion of Fig. 7, the available single interferometric electric signal is concentrated in tens of microseconds. Theoretically, the single-shot acquisition time is effectively reduced within 100 ms at an optical resolution better than tens of picometers with such an approach. With this advantage, the optical response of PFBG is carefully measured at different temperature setting points, which range from 5 to 60 °C at a step resolution of 2.5 °C. Single-shot acquisition is accomplished within 100 μ s with a 6.3 GHz apodized optical resolution at a refresh rate of 180 Hz. 1000 times averaging of the Fourier-transformed spectra is adopted for high SNR. Due to the narrow transmission windows at the reflection band of PFBG, a simple algorithm for defining the center positions of the peaks is also applied. The narrow comb-line resolved transmission peak in optical profiles of PFBG is enlarged as shown in the red part of Fig. 9. The peaks of comb lines are extracted with black “x” marks. The green line illustrates the curve of peaks obtained based on Gaussian fitting. The points of m_1 and m_2 on the curve are at half maximum of the transmitted peak. Here, the midpoint of m_1 and m_2 represents the radio-frequency position of the PFBG center peak. The relationship between temperature variations and radio-frequency positions of the PFBG center peak can be attained by tuning the temperature settings (Fig. 10).

Because of the limitation of the TEC device, the maximum temperature variation ranges from 5 to

60 °C (Fig. 10). However, the optical spectral bandwidth of the measurement exceeds 14 nm. The thermal damage threshold of the fiber guarantees a large dynamic range. During temperature tuning, the gain is about 4.091 kHz/°C. A higher optical resolution of 6.3 MHz is also studied during slight temperature tuning around 21 °C, as shown in the insertion of Fig. 10. However, the gain is reduced to 3.8 kHz/°C, which is closer to the real value with higher resolution.

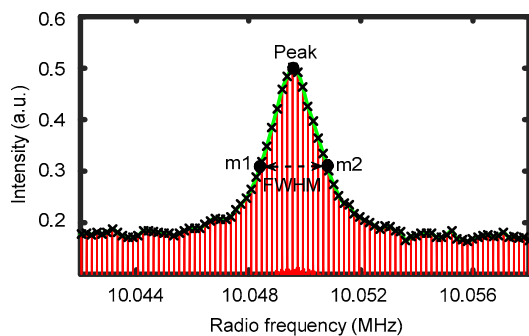


Fig. 9 Narrow windows of PFBG

References to color refer to the online version of this figure

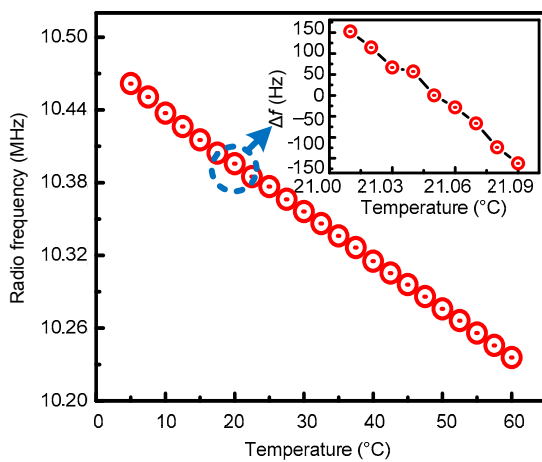


Fig. 10 Relationship between radio-frequency positions and temperature settings with an optical resolution of 6 GHz (insertion: 6.3 MHz)

To evaluate the systematic error in the measurement of the PFBG's center frequency, we performed a stability measurement of the PFBG transmission frequency while keeping the ambient temperature constant. We maintained the TEC temperature at 23 °C per day and measured one state point per day. The number of single sampling points is 96 000. The total measurement time was 35 d. The movement of the PFBG's center frequency is shown in Fig. 11.

Because the ambient temperature was not changed, the instantaneous transmission frequency should be constant. However, we observed a tiny transmission frequency fluctuation. This could be due to AM noise in the optical frequency combs, which may couple to the center frequency shift in the data analysis process. Alternatively, due to the limitations of our temperature isolation conditions, although the TEC temperature can be controlled, the ambient temperature will also have a certain impact. It can be seen from the figure that the frequency jitter range is within 90 Hz and that the ambient temperature change is 0.02 °C.

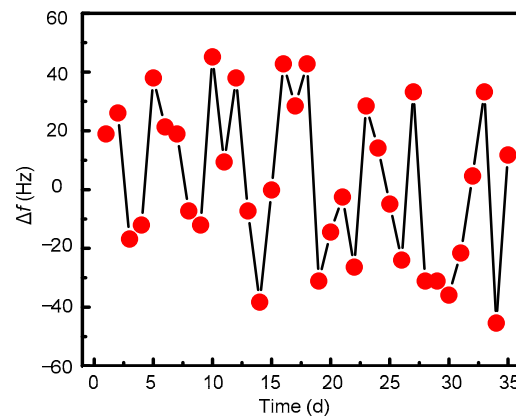


Fig. 11 PFBG center reflection peak stability measurement

4 Conclusions

In conclusion, advantages from dual-comb system are retained in the adaptive sampling system, including broader spectra, high resolution, and fast acquisition speed. Furthermore, it will be applicable in outdoor applications without high demands on long-term coherence between combs. Fast instabilities between comb lines are well compensated for without extra tight phase-locking of combs. It holds much promise in practical outdoor applications due to the only requirements of loose stabilization for long-term measurements. We demonstrate that rapid thermal sensing is realized in high resolution by precise measurements of optical frequency shifts of a PFBG in the radio-frequency domain with adaptive sampling techniques. Given the resolution requirements in different applications, flexible resolution setting from 0.1 to 10 pm in optical level depends on a short acquisition time ranging from tens of micro-

seconds to several seconds. Linear relationship between the optical response of PFBG and the temperature is also characterized by interrogation with ADCS. The optical spectral bandwidth of the measurement exceeds 14 nm. It indicates that the large dynamic temperature range is limited by the temperature damage threshold of the fiber.

References

- Bernhardt B, Ozawa A, Jacquet P, et al., 2010. Cavity-enhanced dual-comb spectroscopy. *Nat Photon*, 4(1): 55-57. <https://doi.org/10.1038/nphoton.2009.217>
- Cassinerio M, Gambetta A, Coluccelli N, et al., 2014. Absolute dual-comb spectroscopy at 1.55 μm by free-running Er:fiber lasers. *Appl Phys Lett*, 104(23):231102. <https://doi.org/10.1063/1.4882862>
- Chow JH, McClelland DE, Gray MB, et al., 2005. Demonstration of a passive submicrostrain fiber strain sensor. *Opt Lett*, 30(15):1923-1925. <https://doi.org/10.1364/OL.30.001923>
- Coddington I, Swann WC, Newbury NR, 2008. Coherent multiheterodyne spectroscopy using stabilized optical frequency combs. *Phys Rev Lett*, 100(1):013902. <https://doi.org/10.1103/PhysRevLett.100.013902>
- Coddington I, Swann WC, Newbury NR, 2009. Coherent linear optical sampling at 15 bits of resolution. *Opt Lett*, 34(14):2153-2155. <https://doi.org/10.1364/OL.34.002153>
- Coddington I, Swann WC, Newbury NR, 2010. Coherent dual-comb spectroscopy at high signal-to-noise ratio. *Phys Rev A*, 82(4):043817. <https://doi.org/10.1103/PhysRevA.82.043817>
- Coddington I, Newbury N, Swann W, 2016. Dual-comb spectroscopy. *Optica*, 3(4):414-426. <https://doi.org/10.1364/OPTICA.3.000414>
- Cusano A, Cutolo A, Nasser J, et al., 2004. Dynamic strain measurements by fibre Bragg grating sensor. *Sens Act A*, 110(1-3):276-281. <https://doi.org/10.1016/j.sna.2003.10.031>
- Deng YJ, Lu F, Knox WH, 2005. Fiber-laser-based difference frequency generation scheme for carrier-envelope-offset phase stabilization applications. *Opt Expr*, 13(12): 4589-4593. <https://doi.org/10.1364/OPEX.13.004589>
- Deschênes JD, Giaccari P, Genest J, 2010. Optical referencing technique with CW lasers as intermediate oscillators for continuous full delay range frequency comb interferometry. *Opt Expr*, 18(22):23358-23370. <https://doi.org/10.1364/OE.18.023358>
- Diddams SA, 2010. The evolving optical frequency comb. *J Opt Soc Am B*, 27(11):B51-B62. <https://doi.org/10.1364/JOSAB.27.000B51>
- Droste S, Ycas G, Washburn BR, et al., 2016. Optical frequency comb generation based on Erbium fiber lasers. *Nanophoton*, 5(2):196-213. <https://doi.org/10.1515/nanoph-2016-0019>
- Du WC, Tao XM, Tam HY, 1999. Fiber Bragg grating cavity sensor for simultaneous measurement of strain and temperature. *IEEE Photon Technol Lett*, 11(1):105-107. <https://doi.org/10.1109/68.736409>
- Gagliardi G, Salza M, Avino S, et al., 2010. Probing the ultimate limit of fiber-optic strain sensing. *Science*, 330(6007):1081-1084. <https://doi.org/10.1126/science.1195818>
- Giaccari P, Deschênes JD, Saucier P, et al., 2008. Active Fourier-transform spectroscopy combining the direct RF beating of two fiber-based mode-locked lasers with a novel referencing method. *Opt Expr*, 16(6):4347-4365. <https://doi.org/10.1364/OE.16.004347>
- Hao Q, Wang YF, Luo P, et al., 2017. Self-starting drop-out-free harmonic mode-locked soliton fiber laser with a low timing jitter. *Opt Lett*, 42(12):2330-2333. <https://doi.org/10.1364/OL.42.002330>
- He ZY, Liu QW, Tokunaga T, 2012. Realization of nano-strain-resolution fiber optic static strain sensor for geo-science applications. Proc Conf on Lasers and Electro-Optics. p.1-2
- Hugi A, Villares G, Blaser S, et al., 2012. Mid-infrared frequency comb based on a quantum cascade laser. *Nature*, 492(7428):229-233. <https://doi.org/10.1038/nature11620>
- Ideguchi T, Poisson A, Guelachvili G, et al., 2012. Adaptive dual-comb spectroscopy in the green region. *Opt Lett*, 37(23):4847-4849. <https://doi.org/10.1364/OL.37.004847>
- Ideguchi T, Poisson A, Guelachvili G, et al., 2014. Adaptive real-time dual-comb spectroscopy. *Nat Commun*, 5:3375. <https://doi.org/10.1038/ncomms4375>
- Ideguchi T, Nakamura T, Kobayashi Y, et al., 2016. Kerr-lens mode-locked bidirectional dual-comb ring laser for broadband dual-comb spectroscopy. *Optica*, 3(7):748-753. <https://doi.org/10.1364/OPTICA.3.000748>
- Jin YW, Cristescu SM, Harren FJM, et al., 2015. Femtosecond optical parametric oscillators toward real-time dual-comb spectroscopy. *Appl Phys B*, 119(1):65-74. <https://doi.org/10.1007/s00340-015-6035-y>
- Keilmann F, Gohle C, Holzwarth R, 2004. Time-domain mid-infrared frequency-comb spectrometer. *Opt Lett*, 29(13): 1542-1544. <https://doi.org/10.1364/OL.29.001542>
- Kersey AD, Berkoff TA, Morey WW, 1993. Multiplexed fiber Bragg grating strain-sensor system with a fiber Fabry-Perot wavelength filter. *Opt Lett*, 18(16):1370-1372. <https://doi.org/10.1364/OL.18.001370>
- Kourogi M, Nakagawa K, Ohtsu M, 1993. Wide-span optical frequency comb generator for accurate optical frequency difference measurement. *IEEE J Quant Electron*, 29(10):2693-2701. <https://doi.org/10.1109/3.250392>
- Kuse N, Ozawa A, Kobayashi Y, 2012. Comb-resolved dual-comb spectroscopy stabilized by free-running continuous-wave lasers. *Appl Phys Expr*, 5(11):112402. <https://doi.org/10.1143/APEX.5.112402>
- Kuse N, Ozawa A, Kobayashi Y, 2013. Static FBG strain sensor with high resolution and large dynamic range by dual-comb spectroscopy. *Opt Expr*, 21(9):11141-11149. <https://doi.org/10.1364/OE.21.011141>
- Lam TTY, Chow JH, Shaddock DA, et al., 2010a. High-resolution absolute frequency referenced fiber optic sensor for quasi-static strain sensing. *Appl Opt*, 49(21):

- 4029-4033. <https://doi.org/10.1364/AO.49.004029>
- Lam TTY, Gagliardi G, Salza M, et al., 2010b. Optical fiber three-axis accelerometer based on lasers locked to π phase-shifted Bragg gratings. *Meas Sci Technol*, 21(9):094010. <https://doi.org/10.1088/0957-0233/21/9/094010>
- Li JM, Ma YC, Yan SB, et al., 2013. High precision and wide scale fiber Bragg grating sensor interrogation system based on tunable filter. *Chin J Lasers*, 40(9):0905002 (in Chinese).
- Majumder M, Gangopadhyay TK, Chakraborty AK, et al., 2008. Fibre Bragg gratings in structural health monitoring—present status and applications. *Sens Actuat A*, 147(1):150-164. <https://doi.org/10.1016/j.sna.2008.04.008>
- Measures RM, 2001. Structural Monitoring with Fiber Optic Technology. Academic Press, San Diego, USA.
- Millot G, Pitois S, Yan M, et al., 2016. Frequency-agile dual-comb spectroscopy. *Nat Photon*, 10(1):27-30. <https://doi.org/10.1038/nphoton.2015.250>
- Newbury NR, Swann WC, 2007. Low-noise fiber-laser frequency combs. *J Opt Soc Am B*, 24(8):1756-1770. <https://doi.org/10.1364/JOSAB.24.001756>
- Newbury NR, Coddington I, Swann W, 2010. Sensitivity of coherent dual-comb spectroscopy. *Opt Expr*, 18(8):7929-7945. <https://doi.org/10.1364/OE.18.007929>
- Rieker GB, Giorgetta FR, Swann WC, et al., 2014. Frequency-comb-based remote sensing of greenhouse gases over kilometer air paths. *Optica*, 5(1):290-298. <https://doi.org/10.1364/OPTICA.1.000290>
- Roy J, Deschênes JD, Potvin S, et al., 2012. Continuous real-time correction and averaging for frequency comb interferometry. *Opt Expr*, 20(20):21932-21939. <https://doi.org/10.1364/OE.20.021932>
- Schiller S, 2002. Spectrometry with frequency combs. *Opt Lett*, 27(9):766-768. <https://doi.org/10.1364/OL.27.000766>
- Schliesser A, Brehm M, Keilmann F, et al., 2005. Frequency-comb infrared spectrometer for rapid, remote chemical sensing. *Opt Expr*, 13(22):9029-9038. <https://doi.org/10.1364/OPEX.13.009029>
- Shen XL, Yan M, Hao Q, et al., 2018. Adaptive dual-comb spectroscopy with 1200-h continuous operation stability. *IEEE Photon J*, 10(5):1503309. <https://doi.org/10.1109/JPHOT.2018.2864986>
- Taurand G, Giaccari P, Deschênes JD, et al., 2010. Time-domain optical reflectometry measurements using a frequency comb interferometer. *Appl Opt*, 49(23):4413-4419. <https://doi.org/10.1364/AO.49.004413>
- Udem T, Holzwarth R, Hänsch TW, 2002. Optical frequency metrology. *Nature*, 416(6877):233-237. <https://doi.org/10.1038/416233a>
- Udem T, Holzwarth R, Hänsch T, 2009. Femtosecond optical frequency combs. *Eur Phys J Spec Top*, 172(1):69-79. <https://doi.org/10.1140/epjst/e2009-01042-6>
- Washburn BR, Diddams SA, Newbury NR, et al., 2004. Phase-locked, erbium-fiber-laser-based frequency comb in the near infrared. *Opt Lett*, 29(3):250-252. <https://doi.org/10.1364/OL.29.000250>
- Wu Q, Semenova Y, Sun A, et al., 2010. High resolution temperature insensitive interrogation technique for FBG sensors. *Opt Laser Technol*, 42(4):653-656. <https://doi.org/10.1016/j.optlastec.2009.11.005>
- Yan M, Luo PL, Iwakuni K, et al., 2017. Mid-infrared dual-comb spectroscopy with electro-optic modulators. *Light Sci Appl*, 6:e17076. <https://doi.org/10.1038/lsa.2017.76>
- Yasui T, Kabetani Y, Saneyoshi E, et al., 2006. Terahertz frequency comb by multifrequency-heterodyning photoconductive detection for high-accuracy, high-resolution terahertz spectroscopy. *Appl Phys Lett*, 88(24):241104. <https://doi.org/10.1063/1.2209718>
- Yasui T, Ichikawa R, Hsieh YD, et al., 2015. Adaptive sampling dual terahertz comb spectroscopy using dual free-running femtosecond lasers. *Sci Rep*, 5:10786. <https://doi.org/10.1038/srep10786>
- Zhang ZW, Gardiner T, Reid DT, 2013. Mid-infrared dual-comb spectroscopy with an optical parametric oscillator. *Opt Lett*, 38(16):3148-3150. <https://doi.org/10.1364/OL.38.003148>
- Zhao X, Hu GQ, Zhao BF, et al., 2016. Picometer-resolution dual-comb spectroscopy with a free-running fiber laser. *Opt Expr*, 24(19):21833-21845. <https://doi.org/10.1364/OE.24.021833>
- Zhu F, Mohamed T, Strohaber J, et al., 2013. Real-time dual frequency comb spectroscopy in the near infrared. *Appl Phys Lett*, 102(12):121116. <https://doi.org/10.1063/1.4799282>
- Zolot AM, Giorgetta FR, Baumann E, et al., 2012. Direct-comb molecular spectroscopy with accurate, resolved comb teeth over 43 THz. *Opt Lett*, 37(4):638-640. <https://doi.org/10.1364/OL.37.000638>